Gamma-response characterization of a solution-grown stilbene based detector assembly in the 59 keV–4.44 MeV energy range; an alternative low-resolution gamma spectrometer

Augusto Di Chicco, Alix Sardet, Michaël Petit, Robert Jacqmin, Vincent Gressier, Brian Stout

Title

Gamma-response characterization of a solution-grown stilbene based detector assembly in the 59 keV - 4.44 MeV energy range; an alternative low-resolution gamma spectrometer

Authors

Augusto Di Chicco[a,d,]
Alix Sardet[b]*
Michaël Petit[c]
Robert Jacqmin[a]
Vincent Gressier[c]
Brian Stout[d]

[a]*CEA, DES, IRESNE, DER*, 13108 Saint-Paul-Lez-Durance CEDEX France
[b]*CEA, DES, IRESNE, DTN, SMTA, LMN*, 13108 Saint-Paul-Lez-Durance CEDEX France
[c] *IRSN Cadarache, SDOS/LMDN,* 13115 Saint-Paul-Lez-Durance, France
[d] *Aix-Marseille University*, Institut Fresnel - UMR 7249, 13397 Marseille, France

***Corresponding Author.** Tel: +33 4 42 25 26 57. E-mail address: Alix.SARDET@cea.fr

Abstract

The photon response characterization of a Ø 25.4 mm × 25.4 mm solution-grown stilbene based detector assembly was performed in the 59 keV - 4.44 MeV energy range. Energy calibration was carried out using not only direct measurements but also via coincidence measurements in order to obtain more reliable results. Both methods gave consistent results. To establish an accurate model of the detector, its energy resolution was determined and included in MCNPX-PoliMi simulations. This model served to compute the gamma-response matrix in the 0.1-7.3 MeV energy range. This matrix was used as an input of the GRAVEL spectrum unfolding code when attempting to unfold the measured spectra of well-known sources. Despite a few discrepancies concerning peak intensities, the main gamma peaks were successfully identified in the 0.059-4.4 MeV energy range, thus confirming the utility of solution-grown stilbene as a low-resolution gamma spectrometer, especially for identifying the gamma component in neutron fields.

Keywords

Organic scintillator detector, solution-grown stilbene, energy calibration, γ-ray response matrix, spectra unfolding, GRAVEL, crystal scintillator, gamma spectrometer.

1 INTRODUCTION

Detectors based on organic scintillators are widely used in the field of fast neutron spectroscopy. Their popularity stems from their high detection efficiencies, sufficient energy resolution, and, for most types, their ability to discriminate neutrons and gamma rays via pulse shape discrimination (PSD) above a minimum threshold. While liquid scintillators, such as BC501A/NE213 [1][2][3], are the most commonly used due to their low production costs and the ease in which they are produced in large volumes, recent developments in solution-growth techniques have made it possible to produce high-quality single organic crystals of various hydrocarbonated compounds at a modest price. These developments revived an interest in crystal scintillators, such as stilbene, to use as neutron spectrometers covering an energy range from ~100 keV [4] to ~20 MeV in order to monitor spectra produced in beam facilities or zero-power experimental nuclear reactors.

The work presented in this paper is part of a larger study dedicated to assessing the neutron spectrometry performance of a Ø 25.4 mm × H 25.4 mm stilbene ($C_{14}H_{12}$) detector assembly. A part of the gamma response, typically between ~340 keV and ~1.550 MeV, must be characterized so that it can be used to calibrate the neutron response. Nevertheless, carrying out a gamma characterization over a wider energy range can also be useful for determining the gamma component accompanying any neutron field.

To this end, two energy calibration techniques, one with direct measurements and one with coincidence measurements, were used to determine the calibration curve. A MCNPX-PoliMi model of the detector was built to help accurately determine the energy resolution of the detector. This model also served to construct the gamma response matrix of the detector, which was then used as an input parameter of the GRAVEL unfolding code for carrying out the deconvolution of experimental spectra of well-known gamma sources.

2 EXPERIMENTAL DETAILS

2.1 ORGANIC SCINTILLATOR DETECTORS

Two cylindrical organic scintillators, listed in Table 1, are used in this work. The main detector is a Ø 25.4 mm × 25.4 mm solution-grown [5] stilbene, produced by InradOptics [6] and encapsulated in a 0.5 mm thick aluminum cylinder. The other detector is only used to perform coincidence measurements and will not be described further. In earlier works [4] [7], the high voltage of the main detector was set to measure low energy neutrons (e.g. -1230 V to measure neutrons below 1 MeV). In the present work, as the goal was to accommodate a neutron energy range as wide as possible (up to 17 MeV), the high voltage was set to -930 V, which corresponds to a gain reduction factor of about 40.

INSERT TABLE 1 HERE

2.2 DATA ACQUISITION AND ANALYSIS

Data acquisition was performed using a CAEN DT5730 digital acquisition (DAQ) system [10], with 8.MCX data acquisition channels, 14-bit resolution, a 2-V maximum digitization window and a 500.MHz sampling rate. Digital acquisition systems offer many advantages compared to analog systems, such as an ease of assembly, the capacity to timestamp at picosecond each triggering signal with a measured 1.ns resolution from DT5730's capability [4], an ability to support high count rates and enhanced neutron/gamma discrimination capabilities [11] [12]. After digitization, anode signals from the photomultipliers are processed by the Digital Pulse Processing - Pulse Shape Discrimination (DPP-PSD) firmware. This firmware timestamps the signals and computes two integrals over two different time-windows: one integral is called Long gate (Q_L) and covers most of the signal, while the other is called Short gate (Q_S) and covers only the fast part of the signal. The ratio of these two integrals provides our PSD information.

The data recorded are: time of radiation detection, Q_L, Q_S, flags (firmware information about the signal recording status) and, if the "wave" mode is selected, the digitized signal itself. This last capacity was not used routinely as it requires considerable computational power, reduces the maximum count rate that the system can handle, and drastically increases data management and analysis requirements. All data produced in this work are processed and analyzed using the ROOT framework [13].

2.3 EXPERIMENTAL SETUPS

In order to perform a complete gamma characterization of the stilbene detector, two sets of experiments were performed using several sources (see Table 2) available at the AMANDE facility [14]. The $^{12}C^*$ first excited state decay of the ^{241}AmBe neutron-gamma source [15] produces 4.438 MeV gamma rays, which primarily interact with the matter through Compton scattering and pair production, thus producing a usable double escape peak at 3.416 MeV and a Compton edge.

INSERT TABLE 2 HERE

2.3.1 Direct measurements

For direct measurement, each gamma source was positioned at 100 mm from the detector front face to ensure a high number of counts in a reasonable amount of time with a relatively homogeneous detector irradiation, while avoiding too many pile-up events.

2.3.2 Coincidence measurements

A known, but seldom-used energy calibration method is based on a gamma scattering coincidence technique [17] [18] [19] [20]. As shown in Figure 1, , for such measurements, the front face of the Ø 25.4 × 25.4 mm^3 stilbene detector was placed at 240 mm from the front face of a Ø 50.8 × 50.8 mm^3 stilbene detector, with their cylindrical axis being aligned. Gamma sources were placed inside a hollow lead cylinder (inner radius of 70 mm), at a distance of around 60 mm below the stilbene crystal, which was thus uniformly irradiated. Since the sources used can emit several gamma simultaneously, lead shielding was used to avoid direct and undesirable coincidences on the second detector. The coincidence window between the two detectors was set to 60 ns. According to the solid angle of the experimental set-up, only gamma rays that interacted with the main stilbene detector with a scattering angle around 90° (within ± 9°) could induce the expected coincidences. The associated uncertainty on the deposited energy varies with the incident gamma ray's energy and reaches a maximum of ~9% around 500 keV (~7% at 1500 keV).

INSERT FIGURE 1 HERE

3 ENERGY CALIBRATION

Energy calibration of a scintillator is performed by associating the known energy of a photoelectric peak, of a Compton Edge (CE) or of simple/double-escape peak to the corresponding discrete channel of the measured spectrum. However, due to the finite energy resolution of the detector, the exact position of the CE is not always easily identifiable. Figure 2 presents the ^{207}Bi (a) and ^{60}Co (b) spectra obtained with the Ø 25.4 × 25.4 mm3 stilbene detector with (red solid line) and without (blue solid line) the coincidence method. Given the experimental setup described in section 2.3, in coincidence mode, each peak is induced by a gamma ray of given energy.

INSERT FIGURE 2 HERE

3.1 DIRECT MEASUREMENTS

In this work, an approach similar to that used to identify the distribution of recoil protons was used [21] to determine the CE position for direct measurements. Indeed, given the shape of the ideal spectrum (sharp drop at the CE position), and irrespective of energy resolution effects, the first-order derivative is assumed to take the form of an inverse Gaussian distribution, centered on the position of the CE (see Figure 3). Such a method was also used in previous works by [22] [23] [24].

INSERT FIGURE 3 HERE

In the energy range between 0.3 MeV and 2 MeV, the relationship between the integral charge (i.e. channel) and the energy deposited by gamma rays is almost linear (see black dashed line on Figure 4(a.1)) [25]. Therefore, the calibration curve, denoted L_{Mean}, can be described using a first-order polynomial:

$$L(MeVee) = b \cdot PH(channel) + a \quad (1)$$

where a and b are parameters determined by fitting the calibration data points. Obtained values are respectively b = (38.59 ± 0.26)×10^{-4} and a = (2.1 ± 0.4)×10^{-2} for a χ^2/ndf[1] of 1.063×10^{-4}/6.

However, for energies below 0.3 MeV and above 2 MeV, a simple linear fit is no longer sufficient to reproduce the stilbene's gamma ray response and a second-order polynomial is considered:

$$L(MeVee) = c \cdot PH^2(channel) + b \cdot PH(channel) + a \quad (2)$$

where *a, b* and *c* are parameters determined by fitting the calibration data points.

At low energy, calibration was performed using data from ^{241}Am as the starting point. This data was completed by a point at 0.344 MeV ($E_{re}(180°)$ = 0.197 MeV), obtained using a ^{152}Eu source. The low-energy calibration curve is denoted L_{Low} (solid red line on Figure 4(a.2)) and its parameters, using the notation from Eq. (2), are a = 0 (imposed value), b = (41.5 ± 0.5)×10^{-4} and c = (-7.77 ± 2.16)×10^{-7}. The associated χ^2/ndf value (1.714×10^{-5}/2) indicates a better data/model agreement than for the previous L_{Mean} result (χ^2/ndf = 4.203×10^{-5}/2 in the same energy range). Similarly, to improve the calibration process at high energy, the double escape peak at 3.416 MeV induced by the 4.438 MeV gamma of $^{12}C^*$ was included in the data set. The associated calibration curve is denoted L_{High} (see blue solid line on Figure 4(a.1)) and its parameters are a = (3.4 ± 0.6)×10^{-2}, b = (38 ± 0.3)×10^{-4} and c = (-9.1 ± 2.8)×10^{-8}. The obtained χ^2/ndf is 2.105×10^{-5}/2, which indicates, even for high energies, a slightly better data/model agreement than for L_{Mean} result (χ^2/ndf = 3.849×10^{-5}/3 in the same energy range).

As can be seen on Figure 4(b), when comparing spectra calibrated using L_{Mean} and L_{High} (resp. L_{Low}), discrepancies are obtained on the CE (resp. photoelectric peak) position. Using L_{Mean}, the 59.6 keV peak of ^{241}Am is overestimated by 33.2% and the 4.196 MeV CE of $^{12}C^*$ by 2%. Therefore, using a purely linear calibration curve (i.e. L_{Mean}) would result in a significant bias in the low (< 0.3 MeV) and a small but real bias in the high (> 2 MeV) energy ranges. The observed non-linearity may have several origins, among which the PMT, the non-linearity of the electron light and the derivative-Gaussian fit method used to determine the CE position. Regarding the latter, comparison to coincidence measurements (see Section 3.2) suggests that it is not the main source of non-linearity.

INSERT FIGURE 4 HERE

3.2 COINCIDENCE MEASUREMENTS

As shown in Figure 2, in coincidence measurements, the recorded spectra take the shape of Gaussian distribution, centered on the energy deposited by gamma rays scattering at 90°. Since the energy of these photons is lower than that of photons scattered at 180° (see Table 2, $E_{re}(90°)$) the calibration point is obtained for lower energies, and thus lower channels, than with a direct measurement.

The main advantage of the coincidence configuration is that, for each source, the peak positions correspond to well-known energies, thus giving a direct calibration curve. As this calibration does not depend on any assumption (for instance the position of the CE), it can be used to assess the accuracy of other calibration methods, such as the derivative method used in the previous section. However, its main drawback is that it requires about 200 times longer measurement times than direct measurements in order to acquire sufficient data for a reliable measurement. Given the available sources (see Table 2), this calibration could only be established for energies below 2 MeV. For energies below 0.3 MeV, the obtained calibration points exhibit the same non-linear behavior as that observed during direct

[1] Ndf (number of degrees of freedom) = number of data points – number of fitting function parameters (for the ROOT framework)

measurements. This proves the cause of the non-linear behavior is not to be found in the used derivative method. A parametrization with a second-order polynomial function below 0.3 MeV and a first-order polynomial up to 2 MeV was used to account for this non-linearity.

3.3 PERFORMANCE COMPARISON OF CALIBRATION METHODS

Calibration curves obtained for direct (black solid square) and coincidence (black empty square) measurements are presented on Figure 5 (left). Corresponding equation parameters are presented in Table 3. Overall, the obtained curves present an excellent agreement with parameters compatible within uncertainties and a maximum deviation of 1.54% at 0.138 MeV. Figure 5 (right) compares the experimental spectrum of ^{60}Co calibrated with (blue solid line) and without (red solid line) the coincidence method. Compared to the reference energies of ^{60}Co, there are shifts of 0.38% and 0.57% at 1.173 MeV and of 0.08% and 0.35% at 1.332 MeV with and without the coincidence method, respectively.

INSERT FIGURE 5 HERE

INSERT TABLE 3 HERE

Results obtained by the direct and coincidence methods are in good agreement and both techniques provide an accurate calibration curve. Since direct measurements are much easier and faster, this approach will be kept for future work.

4 MCNPX SIMULATIONS

To simulate stilbene's gamma ray response, the MCNPX Monte Carlo code has been chosen. It is used in photon-electron mode with the ENDF/B-VI photo-atomic data libraries to define material properties. The constructed geometric model is a simple one, which includes the stilbene crystal, its aluminum container, the Plexiglas light-guide and the PMT container, which was filled only with air. As mentioned in the previous section, organic scintillators have a finite energy resolution, which one must account for in order to perform accurate simulations. To this end, a Gaussian Energy Broadening (GEB) [27] function can be applied to simulation results.

4.1 ENERGY RESOLUTION

The GEB function is expressed as a function of *FWHM*, which is written as:

$$FWHM(E) = L(E) \cdot R(L(E)) = a' + b'\sqrt{E + c'E^2} \quad (3)$$

In Eq.(3), $L(E)$ represents the light-output and $R(L(E))$ the associated energy resolution, *a'*, *b'* and *c'* are parameters. From the empirical formula (1) [28]:

$$R\big(L(E)\big) = \frac{\Delta L(E)}{L(E)} = 1.5 \cdot \frac{L_{1/2} - L_{MAX}}{L_{1/2}} \quad (4)$$

where L_{MAX} corresponds to the energy of the maximum counts (around the Compton edge) and $L_{1/2}$ to the energy where this count is halved, a first estimation of $R(L(E))$ for the different sources listed in Table 2 was performed. Using the Pulse Height (F8) tally of MCNPX, ideal Compton spectra were computed and then convolved using the GEB function parametrized with the results from equation (3). Discrepancies were observed between simulations and experimental spectra, with an overestimation of $R(L(E))$. Therefore, the $R(L(E))$ value was fixed and manually adjusted until a good agreement was

reached between experimental and simulated data at the CE level. Afterwards, to expand $R(L(E))$ over the whole range of interest, data points thus obtained were fitted using the standard function [28]:

$$R(L(E)) = \sqrt{\alpha^2 + \frac{\beta^2}{L(E)} + \left(\frac{\gamma}{L(E)}\right)^2} \quad (5)$$

in which the α, β and γ parameters respectively account for the light transmission from the scintillator to the photocathode, the statistical variation of the photoelectron production mechanism, and the noise contributions of the acquisition system. Eq. (3) and (5) parameters, which are listed in Table 4, were obtained by fitting the experimental data as shown in Figure 6. For the determination of the energy resolution at 4438 keV and referring to [29], we have accounted for an "apparent" resolution of 90 keV (± 4.keV) arising from the Doppler broadening effect.

INSERT FIGURE 6 HERE

INSERT TABLE 4 HERE

4.2 DIRECT MEASUREMENTS SIMULATIONS

Figure 7 presents the comparison between calibrated experimental spectra (blue solid line), after background subtraction, and simulated (black dashed line), accounting for the stilbene's energy resolution, spectra of the ^{22}Na (a) and ^{207}Bi (b) sources. Experimental spectra are in good agreement with simulated results (less than 1% deviation on the position of the CE). Nevertheless, the simulation does not reproduce the experimentally observed Compton continuum. Non-modelled materials, such as the experiment table or the PMT's components, which create backscatter contributions, could explain such a discrepancy.

INSERT FIGURE 7 HERE

4.3 COINCIDENCE MEASUREMENT SIMULATIONS

Since the F8 tally does not enable the selection of gamma rays scattered at a specific angle (90° in this work), a modified version of the code, MCNPX-PoliMi (Polytechnic of Milano) [30], was used instead. Similarly, to the PTRAC option of MCNPX, MCNPX-PoliMi generates an output file that records, for each simulated history, information about collision events within a user-chosen cell. Among the recorded information, the particle type, deposited energy, number of collisions and incident energy of the interacting particle are of interest to our study. These data were processed using the MPPost (MCNPX-Polimi Post-Processor) software, developed by the same team [31], in order to account for the detector response.

Figure 8 shows the comparison between calibrated experimental and simulated broadened spectra of ^{60}Co (a) and ^{152}Eu (b) sources. For both sources, the positions of the energy peaks in the experimental spectra are in good agreement with that of the simulated spectra. However, discrepancies can be observed on either side of the peak tails. A probable cause is that random coincidences and recoil electrons, which are not correctly simulated [32], are not accounted for.

INSERT FIGURE 8 HERE

Despite a few discrepancies, simulated spectra present a good agreement with experimental ones. Table 5 lists the obtained deviations on both the energy and the FWHM for each measured gamma ray. While the recoil electron energy is relatively well reproduced, with a maximum deviation of about 1% at 79.keV, the FHWM presents more significant deviations (up to 7% on the 0.63 MeV gamma ray from the ^{152}Eu source). The most probable origin of these discrepancies is the simplified model of the

experiment, which does not reproduce the background caused by photon scattering, nor an eventual small shift in the source position.

INSERT TABLE 5 HERE

5 GAMMA RESPONSE MATRIX AND SPECTRUM UNFOLDING

5.1 RESPONSE MATRIX CONSTRUCTION AND INTRINSIC EFFICIENCY

For organic scintillators, as for many other detectors, the relationship between the incident particle flux $\phi(E)$ and the measured response PH(L) can be formally expressed as:

$$\mathrm{PH(L)} = \int_0^\infty R(E,L)\phi(E)dE \quad (6)$$

where $R(E,L)$ is the response matrix, *i.e.* the mathematical operator that contains the relevant normalized responses of the organic scintillator in its operational energy range, and thereby accounts for its energy resolution. The gamma-ray response matrix of the stilbene detector was constructed by performing 240 pointwise isotropic gamma simulations, each with 10^9 particles emitted by a source placed at 100 mm from the detector front face. The response matrix was constructed between 100 keV and 7.3 MeV (i.e. 30 keV/bin), each calculation yielding a simulated response between 0 and 8 MeVee, tallied over 1024 bins. It is necessary to point out the calculated response matrix is an ideal one and in practice, the gamma scattering around the detector should be subtracted in order to correctly deduce an incident spectra $\phi(E)$.

The intrinsic gamma-ray efficiency ε(E) curve can be computed from the response matrix according to equation (7):

$$\varepsilon(E_i) = \int_{L_{th}}^{L_M} R(E_i,L)dL \quad (7)$$

where $R(E_i,L)$ is the gamma ray response at the incident energy (E_i). L_M and L_{th} (in MeVee) are respectively the maximum and the threshold light output. Figure 9 shows, for four different threshold values, the calculated gamma efficiency curve of the stilbene up to 3 MeV. Results are in rather good agreement with experimental values obtained with a ^{137}Cs (0.662 MeV) source. Above a 0.1 MeVee threshold, discrepancies observed remain below 1.6%. These discrepancies could be slightly reduced by improving the MCNPX model used to construct the gamma response matrix (*i.e.* by a better reproduction of the Compton continuum).

INSERT FIGURE 9 HERE

5.2 SPECTRA UNFOLDING WITH GRAVEL ALGORITHM

Unfolding (or deconvolution) is a procedure that addresses the inverse problem in Eq. (6), *i.e.* that gives the energy flux $\phi(E)$ which generated the scintillator response *PH(L)*. Over the years, many methods and codes have been developed for this operation [33] [34]. In this work, the iterative code GRAVEL was chosen as it is widely used for unfolding spectra for both gamma rays [1] [35] and neutrons [36] [37]. GRAVEL uses an iterative algorithm based on the nonlinear least-squares method and only yields physically meaningful solutions (*i.e.* an everywhere positive flux). To start the iterative process, GRAVEL needs the experimental spectrum to be unfolded, the response matrix, an input flux (as a first solution to start the iterations), the maximum number of iterations to be performed and a χ^2 target. The code runs until either the maximum number of iterations or the defined χ^2 target value is reached. For all tested spectra, 50000 iterations were performed using a flat (all bins equal to 1) input flux. Tests were performed to ensure that using such an input flux did not yield significant changes in the result compared to what is obtained when using a realistic input flux. The choice of

50000 iterations depends on the fact that for all tested sources they guarantee the minimum and stable χ^2 value.

Gamma spectra unfolded by GRAVEL are compared with known theoretical peaks [16], in terms of peak average energy and emission intensity in order to assess the quality of the performed unfolding. Figure 10 presents the comparison results for $^{12}C^*$ (a) and ^{152}Eu (b). Experimental spectra were scaled to match the peak of highest emission intensity. Observed deviations on the peak energies and their emission intensities are reported in Table 6.

INSERT FIGURE 10 HERE

INSERT TABLE 6 HERE

For $^{12}C^*$, there is a deviation of 0.24% between the measured and theoretical energies. In addition, sporadic peaks are present at lower energies, probably caused by gamma scattering around the detector. For ^{152}Eu, given the large number of energetically-close gamma lines (over 40 lines of similar intensities in the [0.45-0.7] MeV range for example) and the finite resolution of the stilbene detector, only 13 lines above 1% intensity could be considered. Indeed GRAVEL algorithm can't, in this case, unfold properly low intensity gamma rays which are too energetically-close. In this study, the limit is around 1%. Moreover, in the intervals 0.411-0.444 MeV, 1.085-1.112 MeV and 1.212-1.299 MeV, measurements are compared to the average of the theoretical peaks, weighted by their respective intensities, as the resolution of the detector was not good enough to separate the contributions. While deviations from the expected mean energies are less than 1%, deviations on peak intensities can reach up to 87.92% on the peak of lowest energy (0.244 MeV). These deviations are related to both the complexity of ^{152}Eu source and the uncertainties associated to the stilbene response matrix. Nevertheless, unfolding a stilbene gamma spectrum permits, with sufficient accuracy, a peak identification, even for a complex source, thus demonstrating its capacity as a gamma spectrometer.

6 CONCLUSIONS

In this work, the complete gamma characterization of a Ø 25.4 mm × 25.4 mm solution-grown stilbene based detector assembly has been performed. Gamma sources covering an energy range between 0.059 MeV and 4.438 MeV were used to determine the energy resolution of the detector and perform its energy calibration. For the latter, consistent results were obtained between coincidence measurements and direct measurements, thus showing that applying a first-derivative method to determine the position of the Compton edge is accurate and reliable for calibration purposes. Nevertheless, as non-linearities were observed below 0.3 MeV and above 2 MeV, the calibration curve had to be adapted by introducing second-order polynomials in these ranges in order to use the stilbene as a broadband gamma spectrometer. Simulations were performed using a simple MCNPX-PoliMi model. They successfully reproduced the expected detector behavior around the Compton Edge, although the experimental Compton continuum could not be reproduced, probably because of the rather simple MCNP model used. The gamma-ray response matrix of the detector was built and the intrinsic efficiency curve computed for several thresholds. To validate the constructed matrix, spectra of known sources were unfolded using the GRAVEL iterative code. Results showed that the constructed matrix is sufficient to successfully identify the main gamma peaks present in the spectrum in the energy range between 0.059 and 4.4 MeV. These studies have demonstrated the capabilities of stilbene based detectors to serve as a low-resolution gamma spectrometer in the energy range between 0.059 and 4.4 MeV. Future work will focus on the neutron response characterization of this detector assembly, using monoenergetic neutrons produced by the AMANDE facility and a white neutron spectrum produced by the PTB cyclotron [38]. The main objective of these measurements will be to obtain measured [39] [40] and, if possible, the simulated [41] neutron response matrices of the detector assembly to assess its performance as a broadband neutron spectrometer in mixed radiation

fields. In addition, as part of these measurements, anisotropy effects of the stilbene crystal [42] [43] will be investigated in more details as well as their impact on the neutron response.

Acknowledgments

This project has received funding from the European Union's Horizon 2020 research and innovation program under grant agreements N° 847594 (ARIEL) and 847552 (SANDA).

References

[1] H. Klein et S. Neumann, « Neutron and photon spectrometry with liquid scintillation detectors in mixed fields », *Nucl. Instrum. Methods Phys. Res. Sect. Accel. Spectrometers Detect. Assoc. Equip.*, vol. 476, nº 1, p. 132-142, janv. 2002, doi: 10.1016/S0168-9002(01)01410-3.

[2] R. Batchelor, W. B. Gilboy, J. B. Parker, et J. H. Towle, « The response of organic scintillators to fast neutrons », *Nucl. Instrum. Methods*, vol. 13, p. 70-82, août 1961, doi: 10.1016/0029-554X(61)90171-9.

[3] W. R. Burrus et V. V. Verbinski, « Fast-neutron spectroscopy with thick organic scintillators », *Nucl. Instrum. Methods*, vol. 67, nº 2, p. 181-196, janv. 1969, doi: 10.1016/0029-554X(69)90446-7.

[4] A. D. Chicco, M. Petit, R. Jacqmin, V. Gressier, et B. Stout, « Investigation of the neutron-gamma ray discrimination performance at low neutron energy of a solution-grown stilbene scintillator », *EPJ Web Conf.*, vol. 225, p. 04013, 2020, doi: 10.1051/epjconf/202022504013.

[5] N. P. Zaitseva *et al.*, « Neutron detection with single crystal organic scintillators », San Diego, CA, août 2009, p. 744911. doi: 10.1117/12.829870.

[6] « Inrad Optics, Advanced Optical Materials, Design and Manufacturing ». https://www.inradoptics.com/ (consulté le 23 avril 2020).

[7] L. Dioni, V. Gressier, G. Nardin, R. Jacqmin, B. Stout, et M. Sumini, « Tests of a solution-grown stilbene scintillator in mono-energetic neutron beams of 565 keV and 5 MeV », *Nucl. Instrum. Methods Phys. Res. Sect. Accel. Spectrometers Detect. Assoc. Equip.*, vol. 880, p. 210-215, févr. 2018, doi: 10.1016/j.nima.2017.06.048.

[8] « 9214B Series - ET-Enterprises Ltd ». http://et-enterprises.com/products/photomultipliers/product/p9214b-series (consulté le 5 mai 2019).

[9] « 9266B Series - 51 mm Photomultiplier - ET-Enterprises Ltd ». https://et-enterprises.com/products/photomultipliers/product/p9266b-series (consulté le 19 avril 2021).

[10] « DT5730 », *CAEN - Tools for Discovery*. https://www.caen.it/products/dt5730/ (consulté le 5 mai 2019).

[11] R. Aryaeinejad, J. K. Hartwell, et D. F. Spencer, « Comparison Between Digital and Analog Pulse Shape Discrimination Techniques for Neutron and Gamma Ray Separation », in *IEEE Nuclear Science Symposium Conference Record, 2005*, Wyndham El Conquistador Resort, Puerto Rico, 2005, vol. 1, p. 500-504. doi: 10.1109/NSSMIC.2005.1596302.

[12] C. S. Sosa, M. Flaska, et S. A. Pozzi, « Comparison of analog and digital pulse-shape-discrimination systems », *Nucl. Instrum. Methods Phys. Res. Sect. Accel. Spectrometers Detect. Assoc. Equip.*, vol. 826, p. 72-79, août 2016, doi: 10.1016/j.nima.2016.03.088.

[13] « ROOT a Data analysis Framework | ROOT a Data analysis Framework », 6 mai 2019. https://root.cern.ch/ (consulté le 6 mai 2019).

[14] V. Gressier *et al.*, « AMANDE: a new facility for monoenergetic neutron fields production between 2 keV and 20 MeV », *Radiat. Prot. Dosimetry*, vol. 110, nº 1-4, Art. nº 1-4, août 2004, doi: 10.1093/rpd/nch185.

[15] I. Murata, I. Tsuda, R. Nakamura, S. Nakayama, M. Matsumoto, et H. Miyamaru, « Neutron and gamma-ray source-term characterization of AmBe sources in Osaka University », *Prog. Nucl. Sci. Technol.*, vol. 4, p. 345-348, 2014, doi: 10.15669/pnst.4.345.

[16] « NUCLÉIDE-LARA on the web (2020) ». http://www.nucleide.org/Laraweb/index.php

[17] R. Cherubini, G. Moschini, R. Nino, R. Policroniades, et A. Varela, « Gamma calibration of organic scintillators », *Nucl. Instrum. Methods Phys. Res. Sect. Accel. Spectrometers Detect. Assoc. Equip.*, vol. 281, nº 2, p. 349-352, sept. 1989, doi: 10.1016/0168-9002(89)91332-6.
[18] G. Dietze, « Energy calibration of NE-213 scintillation counters by δ-rays », *IEEE Trans. Nucl. Sci.*, vol. 26, nº 1, p. 398-402, févr. 1979, doi: 10.1109/TNS.1979.4329665.
[19] A. A. Naqvi, F. Z. Khiari, A. Coban, A. Aksoy, et A. M. Al-Jalal, « Pulse height resolution of organic scintillators for monoenergetic gamma rays », in *IEEE Conference on Nuclear Science Symposium and Medical Imaging*, oct. 1992, p. 4-6 vol.1. doi: 10.1109/NSSMIC.1992.301166.
[20] Y. Jie, L. Rong, L. Cheng, J. Li, L. Xin-Xin, et Z. Tong-Hua, « Energy calibration of a BC501A liquid scintillator using a γ-γ coincidence technique », *Chin. Phys. C*, vol. 34, nº 7, p. 993-997, juill. 2010, doi: 10.1088/1674-1137/34/7/012.
[21] N. V. Kornilov, I. Fabry, S. Oberstedt, et F.-J. Hambsch, « Total characterization of neutron detectors with a 252Cf source and a new light output determination », *Nucl. Instrum. Methods Phys. Res. Sect. Accel. Spectrometers Detect. Assoc. Equip.*, vol. 599, nº 2-3, p. 226-233, févr. 2009, doi: 10.1016/j.nima.2008.10.032.
[22] L. Stevanato *et al.*, « Light output of EJ228 scintillation neutron detectors », *Appl. Radiat. Isot.*, vol. 69, nº 2, Art. nº 2, févr. 2011, doi: 10.1016/j.apradiso.2010.10.022.
[23] A. Enqvist, C. C. Lawrence, B. M. Wieger, S. A. Pozzi, et T. N. Massey, « Neutron light output response and resolution functions in EJ-309 liquid scintillation detectors », *Nucl. Instrum. Methods Phys. Res. Sect. Accel. Spectrometers Detect. Assoc. Equip.*, vol. 715, p. 79-86, juill. 2013, doi: 10.1016/j.nima.2013.03.032.
[24] H. Wang, D. Carter, T. N. Massey, et A. Enqvist, « Neutron light output function and resolution investigation of the deuterated organic liquid scintillator EJ-315 », *Radiat. Meas.*, vol. 89, p. 99-106, juin 2016, doi: 10.1016/j.radmeas.2016.03.009.
[25] K. F. Flynn, L. E. Glendenin, E. P. Steinberg, et P. M. Wright, « Pulse height-energy relations for electrons and alpha particles in a liquid scintillator », *Nucl. Instrum. Methods*, vol. 27, nº 1, p. 13-17, avr. 1964, doi: 10.1016/0029-554X(64)90129-6.
[26] R. A. Weldon, J. M. Mueller, P. Barbeau, et J. Mattingly, « Measurement of EJ-228 plastic scintillator proton light output using a coincident neutron scatter technique », *Nucl. Instrum. Methods Phys. Res. Sect. Accel. Spectrometers Detect. Assoc. Equip.*, vol. 953, p. 163192, févr. 2020, doi: 10.1016/j.nima.2019.163192.
[27] D. B. Pelowitz *et al.*, « MCNPX 2.7.0 extensions », LA-UR-11-02295, LA-UR-11-2295, 1058045, avr. 2011. doi: 10.2172/1058045.
[28] G. Dietze et H. Klein, « Gamma-calibration of NE 213 scintillation counters », *Nucl. Instrum. Methods Phys. Res.*, vol. 193, nº 3, p. 549-556, mars 1982, doi: 10.1016/0029-554X(82)90249-X.
[29] Z. Janout, S. Pospíšil, et M. Vobecký, « Observation of a Doppler broadening of the 4438 keV gamma-line of12C in processes 12C(n, n′γ)12C and 9Be(α, nγ)12C », J. Radioanal. Chem., vol. 56, no 1, p. 71-81, mars 1980, doi: 10.1007/BF02516939.
[30] S. A. Pozzi, E. Padovani, et M. Marseguerra, « MCNP-PoliMi: a Monte-Carlo code for correlation measurements », *Nucl. Instrum. Methods Phys. Res. Sect. Accel. Spectrometers Detect. Assoc. Equip.*, vol. 513, nº 3, Art. nº 3, nov. 2003, doi: 10.1016/j.nima.2003.06.012.
[31] E. C. Miller, S. D. Clarke, M. Flaska, S. Prasad, S. A. Pozzi, et E. Padovani, « MCNPX-PoliMi Post-Processing Algorithm for Detector Response Simulations », p. 10.
[32] C. B. Sivels, S. D. Clarke, E. Padovani, A. M. Prinke, J. I. McIntyre, et S. A. Pozzi, « Validation of MCNPX-PoliMi code for simulations of radioxenon beta–gamma coincidence detection », *Nucl. Instrum. Methods Phys. Res. Sect. Accel. Spectrometers Detect. Assoc. Equip.*, vol. 906, p. 43-49, oct. 2018, doi: 10.1016/j.nima.2018.07.089.
[33] M. Matzke, « Unfolding procedures », *Radiat. Prot. Dosimetry*, vol. 107, nº 1-3, p. 155-174, nov. 2003, doi: 10.1093/oxfordjournals.rpd.a006384.
[34] M. Reginatto, « Overview of spectral unfolding techniques and uncertainty estimation », *Radiat. Meas.*, vol. 45, nº 10, p. 1323-1329, déc. 2010, doi: 10.1016/j.radmeas.2010.06.016.
[35] X. Xie, X. Yuan, X. Zhang, T. Fan, J. Chen, et X. Li, « Calibration and Unfolding of the Pulse Height Spectra of Liquid Scintillator-Based Neutron Detectors Using Photon Sources », *Plasma Sci. Technol.*, vol. 14, nº 6, p. 553-557, juin 2012, doi: 10.1088/1009-0630/14/6/27.

[36] H. Klein, « Neutron spectrometry in mixed fields: NE213/BC501A liquid scintillation spectrometers », *Radiat. Prot. Dosimetry*, vol. 107, nº 1-3, p. 95-109, nov. 2003, doi: 10.1093/oxfordjournals.rpd.a006391.
[37] Y. Chen *et al.*, « Unfolding the fast neutron spectra of a BC501A liquid scintillation detector using GRAVEL method », *Sci. China Phys. Mech. Astron.*, vol. 57, nº 10, p. 1885-1890, oct. 2014, doi: 10.1007/s11433-014-5553-7.
[38] W. Dep. 6, « Cyclotron », 27 avril 2016. https://www.ptb.de/cms/en/ptb/fachabteilungen/abt6/fb-64/641-ion-accelerators/cyclotron.html (consulté le 4 janvier 2021).
[39] A. Öhrn *et al.*, « Calibration procedure for a neutron monitor at energies below 20MeV », *Nucl. Instrum. Methods Phys. Res. Sect. Accel. Spectrometers Detect. Assoc. Equip.*, vol. 592, nº 3, p. 405-413, juill. 2008, doi: 10.1016/j.nima.2008.04.030.
[40] C. C. Lawrence, M. Febbraro, T. N. Massey, M. Flaska, F. D. Becchetti, et S. A. Pozzi, « Neutron response characterization for an EJ299-33 plastic scintillation detector », *Nucl. Instrum. Methods Phys. Res. Sect. Accel. Spectrometers Detect. Assoc. Equip.*, vol. 759, p. 16-22, sept. 2014, doi: 10.1016/j.nima.2014.04.062.
[41] H. Bai *et al.*, « Simulation of the neutron response matrix of an EJ309 liquid scintillator », *Nucl. Instrum. Methods Phys. Res. Sect. Accel. Spectrometers Detect. Assoc. Equip.*, vol. 886, p. 109-118, avr. 2018, doi: 10.1016/j.nima.2017.12.072.
[42] R. A. Weldon *et al.*, « Characterization of stilbene's scintillation anisotropy for recoil protons between 0.56 and 10 MeV », *Nucl. Instrum. Methods Phys. Res. Sect. Accel. Spectrometers Detect. Assoc. Equip.*, vol. 977, p. 164178, oct. 2020, doi: 10.1016/j.nima.2020.164178.
[43] W. Steinberger, N. Giha, M. Hua, S. Clarke, et S. Pozzi, « Anisotropic neutron response of trans-stilbene and impact on a handheld dual particle imager », *Nucl. Instrum. Methods Phys. Res. Sect. Accel. Spectrometers Detect. Assoc. Equip.*, vol. 1003, p. 165266, juill. 2021, doi: 10.1016/j.nima.2021.165266.

Captions with figures sizes

Figure 1 (Full color online): Picture of the coincidence experimental set-up.

(Size H 83.3 mm L 140)

Figure 2 (Full color online): Comparison between the experimental spectra with (w: red solid line) and without (w/o: blue solid line) the coincidence method for: ^{207}Bi (a) and ^{60}Co (b).

(Size H 74.4 mm L 190 mm)

Figure 3: Normalized and smoothed response given by ^{137}Cs (black square) and its first order derivate (white square). The intersection between the experimental spectrum and the dotted line representing the centroid of the Gaussian distribution indicates the assumed CE position.

(Size H 70.1 mm L 85 mm)

Figure 4 (Full color online): Comparison of the energy calibration curves for high (a.1) and low (a.2) gamma energies; the larger error bars's size is comparable with the symbol one. (b.1) Comparison between ^{12}C* experimental calibrated spectra using L_{Mean} (black solid line) and L_{High} (blue solid line). (b.2) Comparison between ^{241}Am experimental calibrated spectra using L_{Mean} (black solid line) and L_{Low} (red solid line) and the simulated spectrum (blue dashed line) using MCNPX (see Section 4).

(Size H 180.5 mm L 185 mm)

Figure 5 (Full color online): (Left) Comparison of the stilbene calibration data points obtained without (w/o: black solid square) and with (w: black empty square) the coincidence method; the larger error bars's size is comparable with the symbol one. Calibration points have been fitted using Eq. (1) (dashed line) in the energy range between 0.3 and 2 MeV and Eq. (2) (solid line) in the energy range between 0 and 0.3 MeV. For the calibration curves color is used: red for the curve obtained with the coincidence method and blue without it. (Right) Comparison between experimental calibrated spectra for ^{60}Co using L_{Mean} parameters obtained with (blue solid line) and without (red solid line) the coincidence data.

(Size H 80.3 mm L 190 mm)

Figure 6: Energy resolution (a) curve of the stilbene obtained using Eq. (5). FWHM (b) curve of the stilbene obtained using Eq. (3) (black solid line) and $a\cdot\sqrt{E}$ (black dashed line) with $a = (8.12 \pm 0.51)\times10^{-2}$. For both data sets, the larger error bars's size is comparable with the symbol one.

(Size H 79.6 mm L 185 mm)

Figure 7 (Full color online): Comparison between simulated (dashed black line) and experimental calibrated (solid blue line) spectra for ^{22}Na (a) and ^{207}Bi (b).

(Size H 77 mm L 190 mm)

Figure 8 (Full color online): Comparison between the experimental spectrum found with the coincidence method and the corresponding simulated spectra obtained with MCNPX-Polimi for: ^{60}Co (a) and ^{152}Eu (b).

(Size H 77 mm L 190 mm)

Figure 9 (Full color online): Calculated efficiency curves, according to Eq. (7), for Ø25.4 × 25.4 mm^3 stilbene with several thresholds (solid lines). Experimental efficiencies were obtained with a source of ^{137}Cs (black solid squares).

(Size H 77 mm L 85 mm)

Figure 10: Full color online): Comparison between the stilbene unfolded spectra and the expect gamma peaks for: $^{12}C^*$ (a) and ^{152}Eu (b).

(Size H 77 mm L 190 mm)

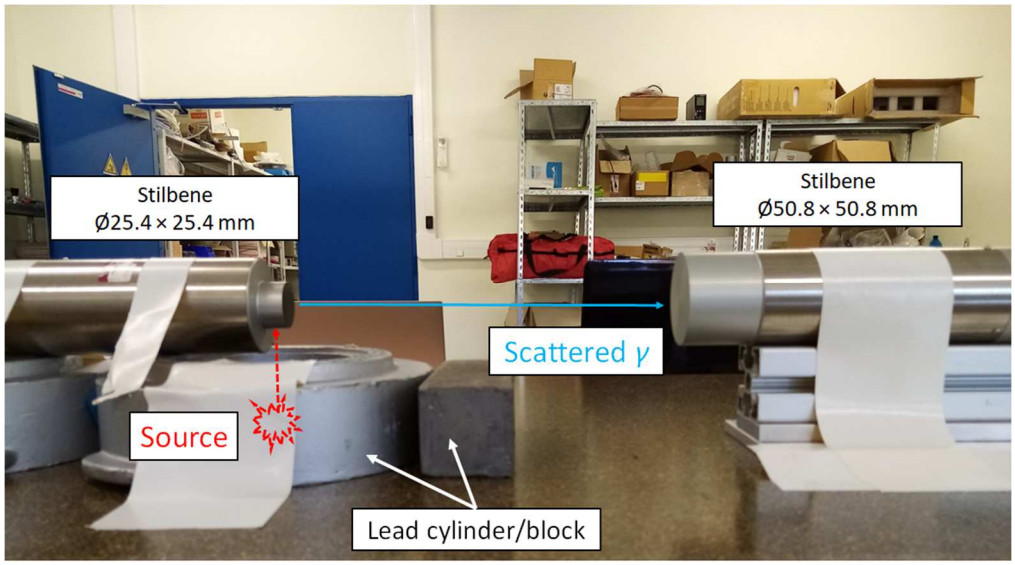

Figure 1

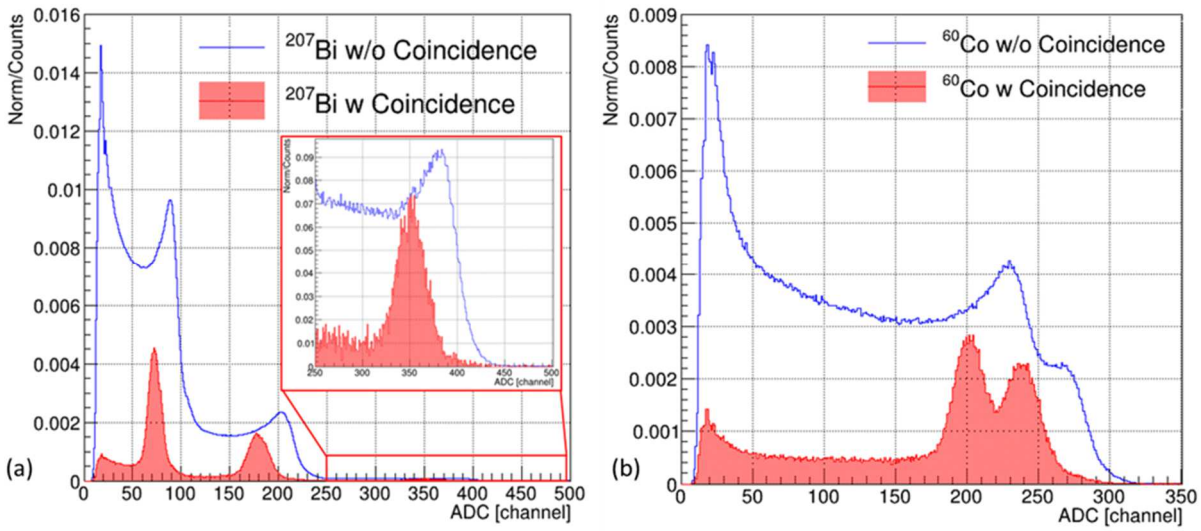

Figure 2

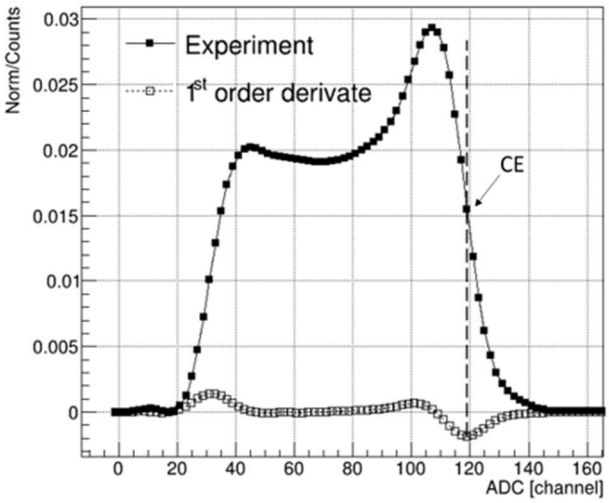

Figure 3

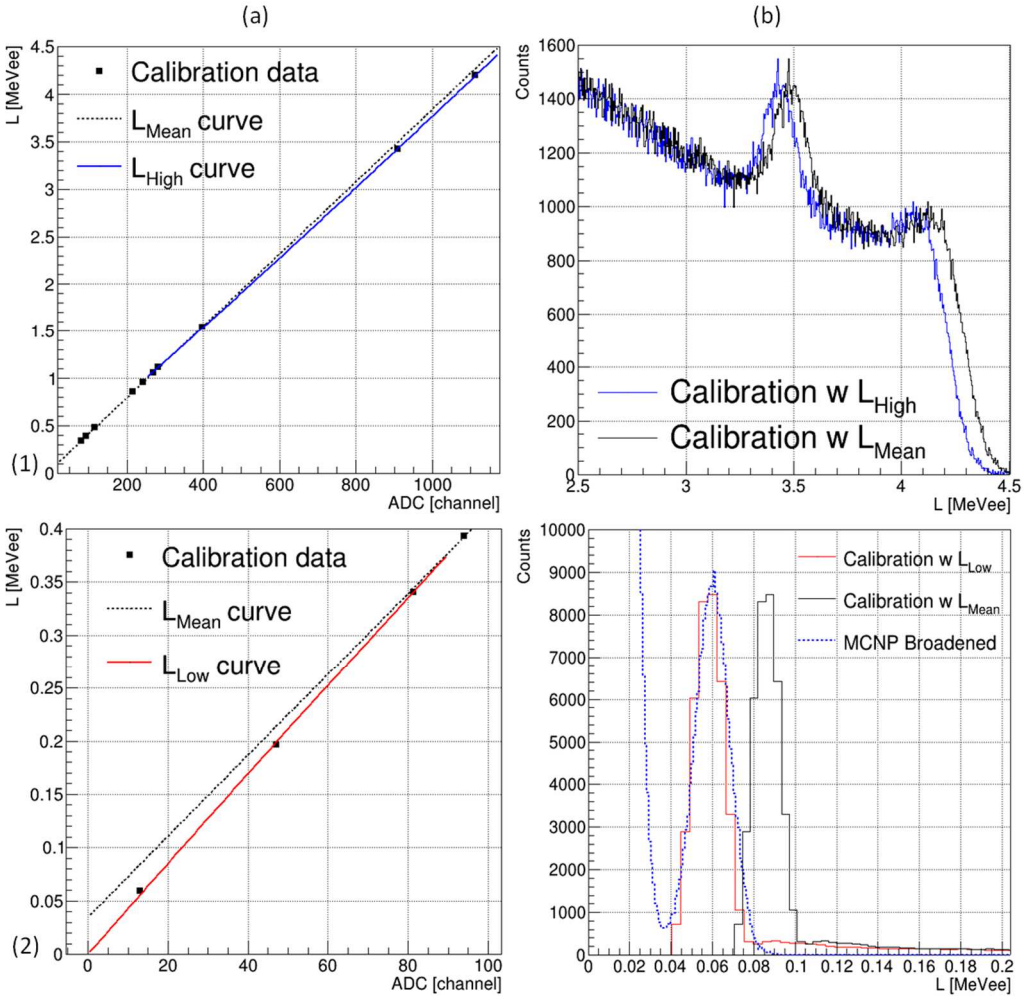

Figure 4

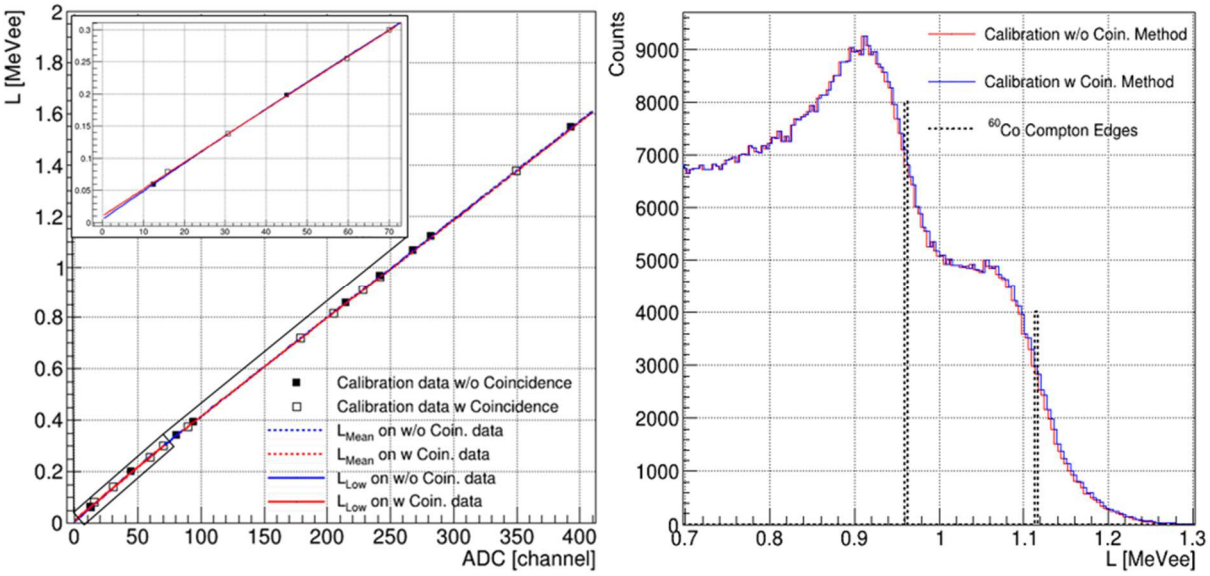

Figure 5

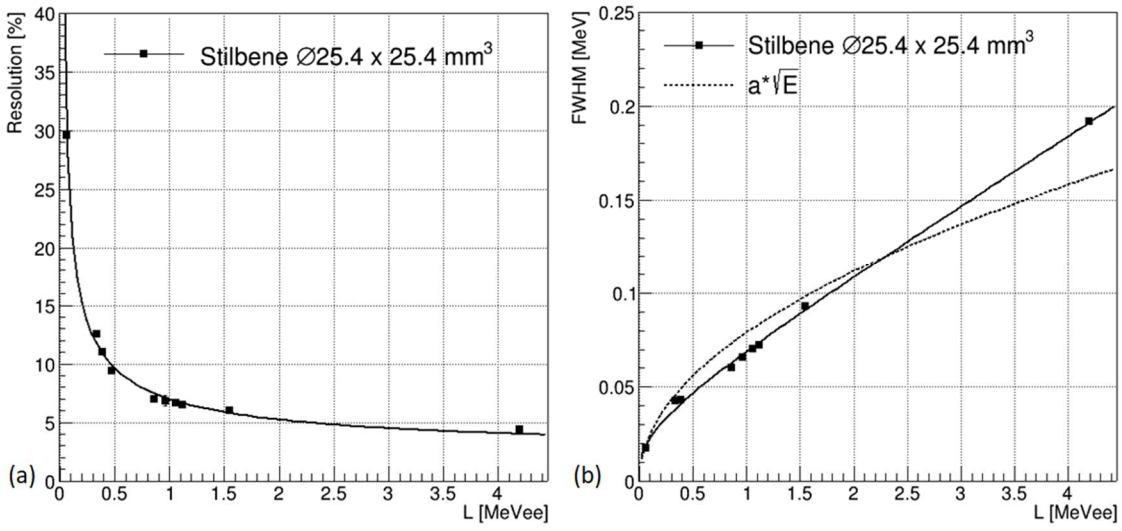

Figure 6

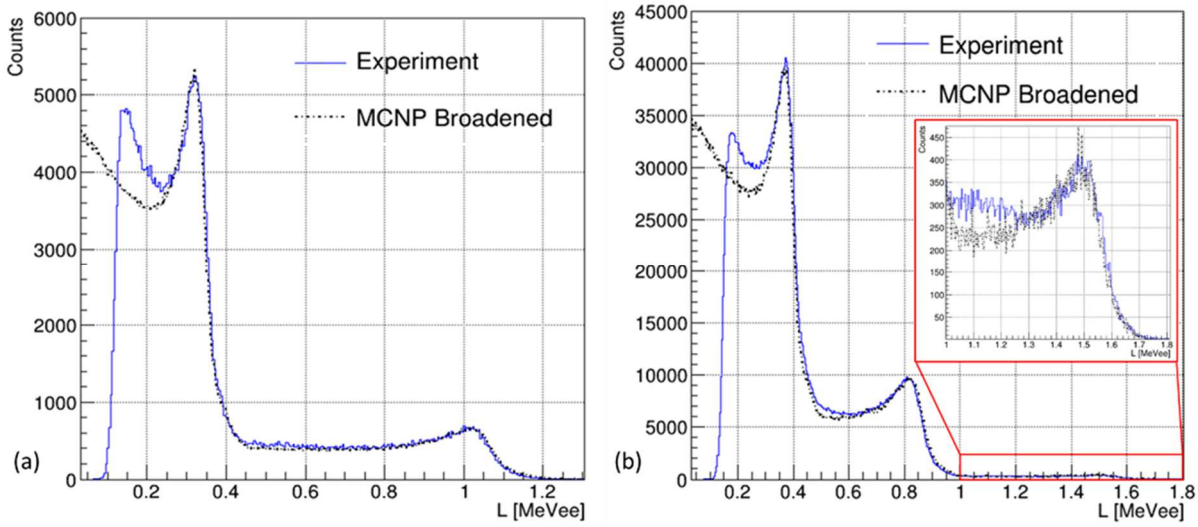

Figure 7

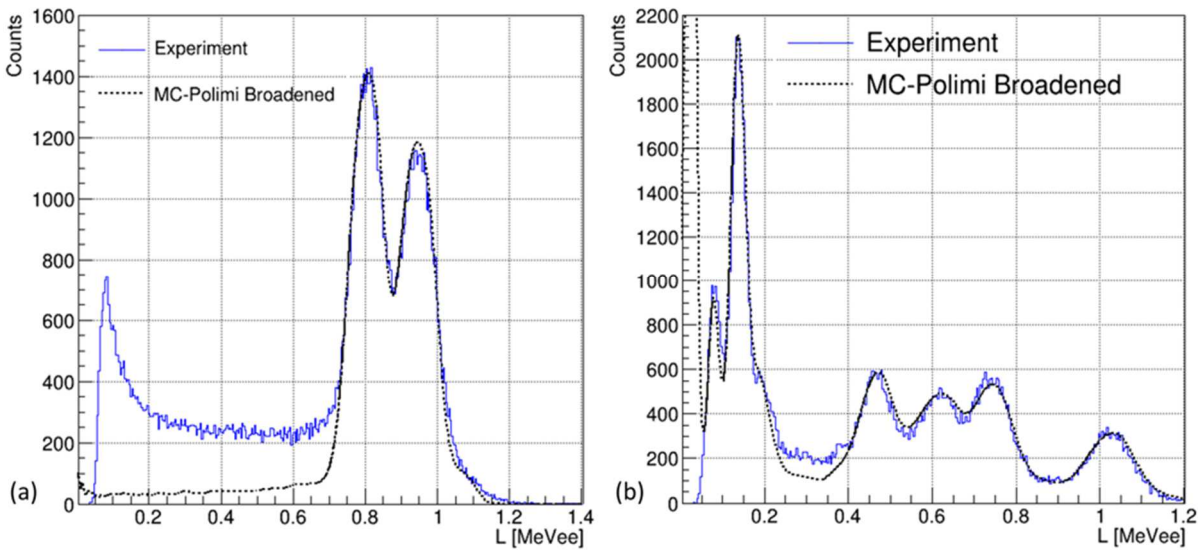

Figure 8

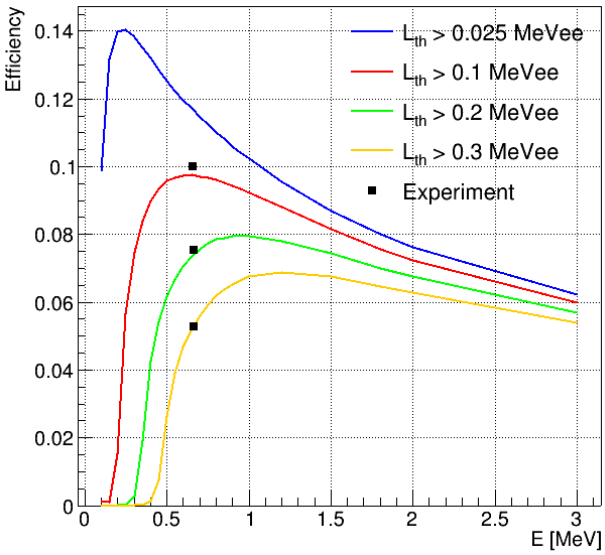

Figure 9

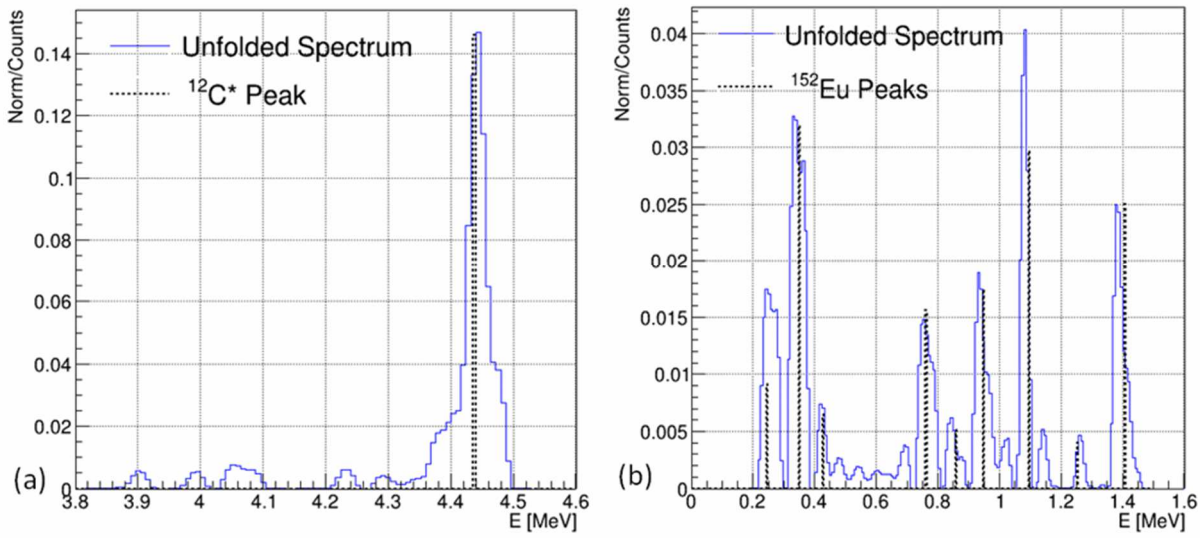

Figure 10

Tables

Table 1: Characteristics of organic scintillators used in this work. The grey line indicates the stilbene detector under study.

Organic scintillator model	Type	Diameter [mm]	Length [mm]	Density [g/cm^3]	Photomultiplier model	Photomultiplier's voltage [V]
Stilbene	Crystal	25.4	25.4	1.15	ET-9214B [8]	-930
Stilbene	Crystal	50.8	50.8	1.15	ET-9266B [9]	-1100

Table 2: Gamma radionuclides used for the stilbene energy calibration, E_γ corresponds to the energy peaks produced by the sources, while E_{re} is the Compton edge energy (180° or 90° recoil electrons). Peak intensities were taken from the LARA library [16]. Sources with a grey background were used in coincidence measurements.

Source	E_γ [keV]	E_{re}(180°) [keV]	E_{re}(90°) [keV]	Intensity [%]	Source activity [kBq]
^{241}Am	59.6	Photoelectric interaction		35.92	-
^{137}Cs	662	478	373	84.99	422.3
^{22}Na	1275 511	1062 341	910 256	99.94 180.7	421
^{60}Co	1332 1173	1117 963	962 817	99.9826 99.85	387.2
^{207}Bi	1770 1063 570	1547 857 394	1374 718 301	6.871 74.58 97.76	384
^{152}Eu	344 244	197 120	138 79	26.5 7.58	480
$^{12}C^*$	4438	4196	3980	85	16.5

Table 3: Stilbene detector calibration parameters with and without the coincidence method for two energy intervals. The L_{Low} parameters are obtained using Eq. (2) while L_{Mean} uses Eq. (1).

	Without the coincidence		With the coincidence	
	L_{Low} [0, 0.3] MeV	L_{Mean} [0.3, 2] MeV	L_{Low} [0, 0.3] MeV	L_{Mean} [0.3, 2] MeV
a	$(0.69 \pm 0.89)\times10^{-2}$	$(2.93 \pm 0.11)\times10^{-2}$	$(0.81 \pm 0.27)\times10^{-2}$	$(2.9 \pm 0.3)\times10^{-2}$
b	$(44.24 \pm 6.57)\times10^{-4}$	$(38.56 \pm 0.04)\times10^{-4}$	$(42.23 \pm 0.65)\times10^{-4}$	$(38.63) \pm 0.17)\times10^{-4}$
c	$(-4.95 \pm 8.71)\times10^{-6}$	-	$(-1.27 \pm 0.24)\times10^{-6}$	-

Table 4: Experimental parameters of equations (5) and (3).

$R(L(E))$			$FWHM(E)$		
α [%]	β [%]	γ [%]	a' [MeV]	b' [MeV $^{1/2}$]	c' [MeV $^{-1}$]
2.4 ± 0.7	6.52 ± 0.27	0.7 ± 0.1	0.006 ± 0.003	0.051 ± 0.005	0.51 ± 0.13

Table 5: Deviations between experimental and simulated spectra for values on the midpoint (E_{re}) and FWHM of Gaussian curves.

Source	$E_{re}(90°)$ [MeV]	E_{re} Deviation	FWHM Deviation
^{152}Eu	0.079	(0.88 ± 0.03)%	(4.98 ± 0.07)%
^{152}Eu	0.138	(0.43 ± 0.01)%	(2.92 ± 0.02)%
^{152}Eu	0.470	(0.52 ± 0.05)%	(2.82 ± 0.11)%
^{152}Eu	0.630	(-0.47 ± 0.11)%	(7.00 ± 0.36)%
^{152}Eu*	0.750	(-0.57 ± 0.08)%	(2.24 ± 0.27)%
^{60}Co	0.817	(-0.27 ± 0.04)%	(1.66 ± 0.14)%
^{60}Co	0.962	(-0.09 ± 0.07)%	(1.59 ± 0.09)%
^{152}Eu	1.033	(-0.40 ± 0.05)%	(3.88 ± 0.01)%

(*The 0.75 MeV measurement corresponds to the average of the 1.085, 1.089 and 1.112 MeV gamma rays, which cannot be separated due to the limited resolution of the detector and of the experimental setup .)

Table 6: Deviation in mean energy value and intensity between the unfolded experimental spectra and theoretical values.

	Gamma Energy (MeV)	Intensity (%)	Mean energy deviation	Intensity deviation
^{152}Eu	0.244	7.55	-0.20%	87.92%
^{152}Eu	0.344	26.59	0.29%	0%
^{152}Eu*	0.4275 (0.411/0.444)	5.358 (2.238/3.12)	0.23%	6.36%
^{152}Eu	0.778	12.97	0.13%	-6.96%
^{152}Eu	0.867	4.24	0.69%	17.03%
^{152}Eu	0.964	14.5	0.73%	5.12%
^{152}Eu*	1.0953 (1.085/1.089/1.112)	25.27 (10.13/1.73/13.41)	0.43%	31.76%
^{152}Eu*	1.2555 (1.212/1.299)	3.04 (1.41/1.63)	-0.83%	7.15%
^{152}Eu	1.408	20.85	0.75%	-2.17%
^{12}C*	4.438	85	-0.24%	-